$$\frac{2}{3}\frac{eF}{\gamma'(2m_n\gamma)^{1/2}}\frac{d}{dE}\gamma f_1(E)$$
$$=-\frac{2}{3}\frac{e^2F^2}{m_n\gamma'(2m_n\gamma)^{1/2}}\frac{d}{dE}\left(\frac{\gamma}{\gamma'}(2m_n\gamma)^{1/2}\tau\frac{df_0}{dE}\right), \quad \text{(A6)}$$

where τ is the relaxation time. Equating (A6) to (A4) and integrating both sides, Eq. (A4), by parts, yields

$$\frac{2}{3}\frac{e^2F^2}{m_n}\frac{\gamma}{\gamma'}(2m_n\gamma)^{1/2}\tau\frac{df_0}{dE}=(\gamma')^2\left(f_0+\eta\frac{df_0}{dE}\right)\left(\sum_n P_nQ_nG_{n1}\right)$$
$$+\int^E(\gamma')^2\left(f_0+\eta\frac{df_0}{dE'}\right)\left(\sum_n\left[P_n\frac{dQ_n}{dE'}-Q_n\frac{dP_n}{dE'}\right]G_{n1}\right)dE'. \quad \text{(A7)}$$

One can now show that the sum over n in the integral term of Eq. (A7) equals zero. The sum over the eight terms for which $P_n\neq Q_n$ gives zero, and for the remainder of the terms, $P_n=Q_n$. One has furthermore

$$\sum P_nQ_nG_{n1}=eF_0k\Theta\int_u^{(4\gamma)^{1/2}}\frac{1}{q}\mathcal{G}(q;E;E)dq$$
$$=eF_0k\Theta\mathcal{G}_1, \quad \text{(A8)}$$

where $\mathcal{G}_1$ is given in the text.

The relaxation time is also readily obtained (compare I), and is given by Eq. (9) of the text; $\mathcal{G}_0$, which is also given there, is

$$\mathcal{G}_0=\frac{1}{2}\int_{-1}^{1}\mathcal{G}(y;E;E)dy.$$

Putting all these equations together, one readily integrates Eq. (A7) to obtain Eq. (8) of the text.

PHYSICAL REVIEW VOLUME 168, NUMBER 3 15 APRIL 1968

de Haas–van Alphen Effect and Fermi Surface of White Tin*

J. E. CRAVEN†
AND
R. W. STARK‡
Department of Physics and the James Franck Institute, The University of Chicago, Chicago, Illinois
(Received 11 August 1967)

We report here the results of an extensive investigation of the de Haas–van Alphen effect in white tin. These results agree qualitatively with the predictions of Weisz's pseudopotential model for the tin Fermi surface; for every case in which Weisz's model differs qualitatively from the single-orthogonalized-plane-wave model, our data agree with the former. Quantitative agreement, however, has not been obtained. The experimentally determined cross-sectional areas of the Fermi surface typically differ by about 30% from those calculated by Weisz. Area branches are also reported that are due to coupled orbits generated by magnetic breakdown of the spin-orbit-coupling-induced energy gap between the third and fourth bands near the XL and XP zone lines.

I. INTRODUCTION

THE electronic properties of metallic ("white") tin have been studied in considerable detail over the past few years. One of the primary reasons for this is the relatively long electron mean free path that can be obtained in pure tin crystals at temperatures of about 1°K. These experimental studies have fallen into two basic categories; those which have used the electronic properties relevant to the Fermi surface to study the Fermi surface itself,[1–18] and those which have studied the purely dynamical aspects of the electronic prop-

* Supported in part by the U. S. Army Research Office (Durham), the National Science Foundation, and the Advanced Research Projects Agency.
† Advanced Research Projects Agency Research Assistant.
‡ Alfred P. Sloan Research Fellow.
[1] A. V. Gold and M. G. Priestley, Phil. Mag. **5**, 1089 (1960).
[2] M. D. Stafleu and A. R. De Vroomen, Phys. Letters **23**, 179 (1966); M. D. Stafleu and A. R. De Vroomen, Phys. Status Solidi **23**, 675 (1967).
[3] N. E. Alekseevskii, Yu. P. Gaidukov, I. M. Lifshitz, and V. G. Peshanskii, Zh. Eksperim. i Teor. Fiz. **39**, 1201 (1960) [English transl.: Soviet Phys.—JETP **12**, 837 (1961)].
[4] N. E. Aledseevskii and Yu. P. Gaidukov, Zh. Eksperim. i Teor. Fiz. **41**, 1079 (1961) [English transl.: Soviet Phys.—JETP **12**, 770 (1962)].
[5] M. S. Khaikin, Zh. Eksperim. i Teor. Fiz. **43**, 59 (1962) [English transl.: Soviet Phys.—JETP **16**, 42 (1963)].
[6] V. F. Gantmakher, Zh. Eksperim. i Teor. Fiz. **44**, 811 (1963) [English transl.: Soviet Phys.—JETP **17**, 549 (1963)].
[7] V. F. Gantmakher and E. A. Kaner, Zh. Eksperim. i Teor. Fiz. **45**, 1430 (1963) [English transl.: Soviet Phys.—JETP **18**, 988 (1964)].
[8] V. F. Gantmakher, Zh. Eksperim. i Teor. Fiz. **45**, 2028 (1964) [English transl.: Soviet Phys.—JETP **19**, 1366 (1964)].
[9] M. S. Khaikin, Zh. Eksperim. i Teor. Fiz. **42**, 27 (1962) [English transl.: Soviet Phys.—JETP **15**, 18 (1963)].
[10] M. S. Khaikin, Zh. Eksperim. i Teor. Fiz. **43**, 59 (1962) [English transl.: Soviet Phys.—JETP **16**, 42 (1963)].
[11] J. F. Koch and A. F. Kip, Phys. Rev. Letters **8**, 473 (1962).
[12] M. S. Khaikin, Zh. Eksperim. i Teor. Fiz. **39**, 513 (1960) [English transl.: Soviet Phys.—JETP **12**, 359 (1961)].
[13] A. A. Galkin, E. A. Kaner, and A. P. Korlyuk, Zh. Eksperim. i Teor. Fiz. **39**, 1517 (1960) [English transl.: Soviet Phys.—JETP **12**, 1055 (1961)].
[14] T. Olsen, J. Phys. Chem. Solids **24**, 649 (1963).
[15] R. J. Kearney, A. R. Mackintosh, and R. C. Young, Phys. Rev. **140**, A1671 (1965).
[16] B. I. Miller, Phys. Rev. **151**, 519 (1966).
[17] E. Fawcett, Proc. Roy. Soc. (London) **A232**, 519 (1955).
[18] R. G. Chambers, Can. J. Phys. **34**, 1395 (1956).

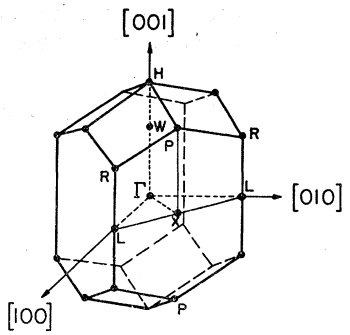

FIG. 1. The first Brillouin zone for white tin together with some of the pertinent symmetry points. The crystallographic [100], [001], and [110] axes are parallel to the ΓL, ΓH, and ΓX zone lines, respectively.

erties.[19–28] The results of both types of experiments could not be interpreted quantitatively without recourse to a precise model for the electronic band structure and Fermi surface of metallic tin.

Recently, however, Weisz[29] utilized pseudopotential techniques to obtain a semiempirical band structure and Fermi-surface model for tin. In doing this, he made extensive use of Ghantmakher's[6,8] beautiful rf size-effect data which measured several of the calipers of the Fermi surface. His resultant model was in fairly good agreement with these calipers. This agreement, however, did not necessarily indicate that his model was correct; the assignments of several of the experimental calipers to various segments of Fermi surface could not be made uniquely. As a check on the consistency of his model, Weisz calculated the extremal cross-sectional areas of his Fermi surface and compared these with the de Haas–van Alphen (dHvA) data of Gold and Priestley.[1] The agreement between these two was not too good; they differed, on the average, by about 20%. This, however, again could not be considered as definitive since the dHvA data were quite incomplete and only suggestive of the general trends. The data were in fact sufficiently incomplete that their assignment to the various sheets of the Fermi surface had to be considered tentative.

[19] A. R. Mackintosh, Phys. Rev. **131**, 2420 (1963).
[20] J. R. Leibowitz, Phys. Rev. **133**, A84 (1964).
[21] B. N. Aleksandrov, Zh. Eksperim. i Teor. Fiz. **43**, 399 (1962) [English transl.: Soviet Phys.—JETP **16**, 286 (1963)].
[22] B. N. Aleksandrov, Zh. Eksperim. i Teor. Fiz. **43**, 1231 (1962) [English transl.: Soviet Phys.—JETP **16**, 871 (1963)].
[23] R. C. Young, Phys. Rev. Letters **15**, 262 (1965).
[24] R. C. Young, Phys. Rev. **152**, 659 (1966).
[25] V. F. Gantmakher and Yu. V. Sharvin, Zh. Eksperim. i Teor. Fiz. **48**, 1077 (1965) [English transl.: Soviet Phys.—JETP **21**, 720 (1965)].
[26] V. B. Zernov and Yu. V. Sharvin, Zh. Eksperim. i Teor Fiz. **36**, 1038 (1959) [English transl.: Soviet Phys.—JETP **9**, 737 (1959)].
[27] Yu. V. Sharvin and V. F. Gantmakher, Zh. Eksperim. i Teor. Fiz. **38**, 1456 (1960). [English transl.: Soviet Phys.—JETP **11**, 1062 (1960)].
[28] V. F. Gantmakher and Yu. V. Sharvin, Zh. Eksperim. i Teor. Fiz. **39**, 1242 (1960 [English transl.: Soviet Phys.—JETP **12**, 358 (1961)].
[29] G. Weisz, Phys. Rev. **149**, 504 (1966).

The purpose of this paper is to report the results of detailed investigations of the dHvA effect in tin. The experimental area branches which are described in this paper are shown to be in excellent *qualitative* agreement with Weisz's model. In every case in which Weisz's model differs qualitatively from the single-OPW (orthogonalized-plane-wave) model our data agree with the former. Thus, in the following discussions we will only consider assignments of the data to the various Fermi-surface sheets of Weisz's model.

II. WEISZ'S FERMI-SURFACE MODEL

White tin crystallizes in the tetragonal crystal structure, the Brillouin zone for which is shown in Fig. 1. The fourfold ΓH line is along the [001] crystal axis; the ΓL and ΓX lines are along the [100] and [110] crystal axes, respectively.

The single-OPW-model Fermi surface has a small pocket of holes in the second band centered near W. Weisz, however, finds that both the first and second bands are completely filled. The third band of the single-OPW model has a set of "pillars" oriented along the XP zone lines and multiply connected by tubes to the region around W. Weisz's model retains the pillars but eliminates the tubes. The resultant surface, shown in Fig. 2(a), has the geometry of a dumbbell centered at point X with twofold axes of rotation along XP (major axis), XL, and $X\Gamma$.

The fourth band of the single-OPW model contains two separate sheets of the Fermi surface both of which are centered on Γ. The larger is an open hole surface consisting of intersecting cylinders whose major axes are along the ΓX lines; the smaller is a closed electron surface which has the geometry of two intersecting convex lenses. Weisz's model, which is shown in Figs. 2(b) and 2(c) retains the general characteristics of the single-OPW model with the exception that the two surface sheets become joined near the ΓH zone line so that there is only one continuous, although reentrant, sheet of the Fermi surface in the fourth band. The portion of this sheet shown in Fig. 2(c) fits within the portion shown in Fig. 2(b), the two being connected by the small, square cross-section neck.

The fifth band of Weisz's model contains an open electron surface consisting of alternately top-up and top-down pear-shaped sections interconnected by a network of tilted tubes. This sheet of the Fermi surface, shown in Fig. 2(d), is similar to the single-OPW model. The fifth band of the single-OPW model also has a cigar-shaped piece centered on Γ. This piece is eliminated in Weisz's model.

The single-OPW model has several cigar-shaped pieces in the sixth band. These are merged into two equivalent sheets centered near W in Weisz's model. Their shape, as shown in Fig. 2(e), strongly resembles an extracted molar.

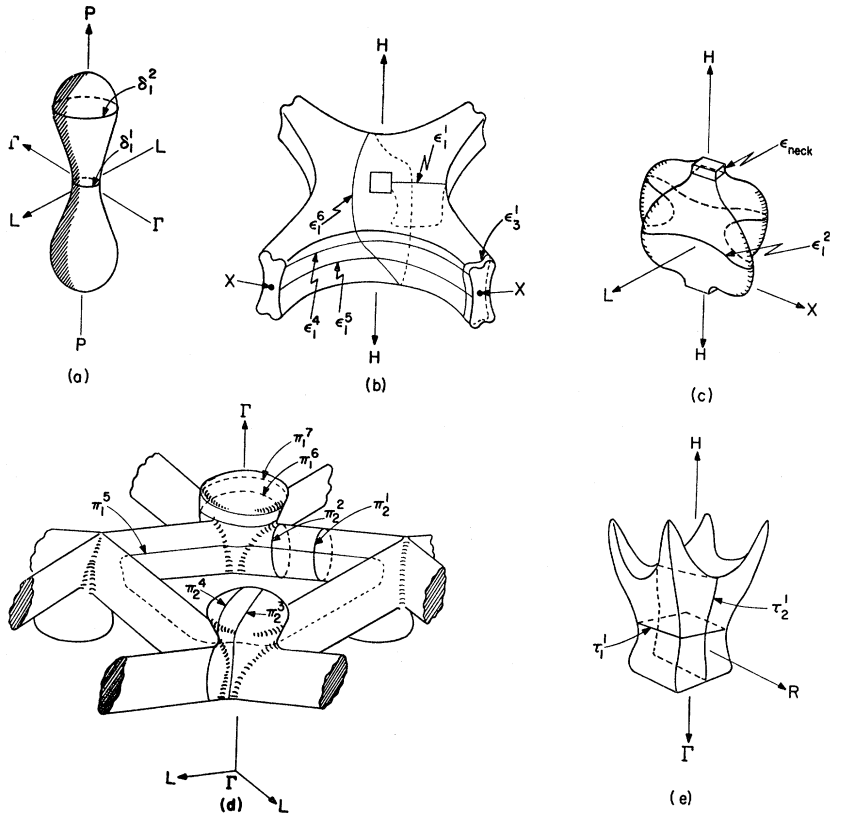

FIG. 2. The various sheets of the Fermi surface according to Weisz's calculation: (a) third-band holes; (b) fourth-band holes; (c) fourth-band electrons (located in the interior of the fourth-band holes); (d) fifth-band electrons; (e) sixth-band electrons. Orbits corresponding to extremal cross sections on each sheet are also shown.

III. EXPERIMENTAL RESULTS

The dHvA measurements were made using large-amplitude field-modulation techniques.[30] Data were taken in fields extending to 38 kG and at temperatures down to 1.1°K. The tin single crystals which were used had residual resistivity ratios of about 40 000.

Figure 3 shows a composite on a semilog scale of all of the primary cross-sectional area branches measured. The absolute accuracy of the experimental area branches is in almost every case better than 1%. The relative accuracy on any single branch as a function of angle is better than 0.1% since nearly all of the data shown in Fig. 3 were obtained using field-rotation diagrams taken at constant magnetic-field strengths. The angle between **H** and [001] is measured by θ when **H** is constrained to move in the (100) and (110) planes; the angle between **H** and [100] is measured by φ when **H** is constrained to move in the (001) plane.

More than forty different area branches are shown in Fig. 3. In addition to these, many more branches were observed but were found to be either harmonics of branches shown in Fig. 3 or sum and difference branches generated by nonlinear coupling of two of the branches shown. Since these branches do not contain any additional information about the cross-sectional areas of the Fermi surface, they are not shown in Fig. 3.

[30] R. W. Stark and L. Windmiller, Cryogenics (to be published).

For simplicity we have adopted the following notation. All area branches assigned to a sheet of the Fermi surface in a given band are denoted by the same Greek letter. Each letter carries a subscript and a superscript. The subscript denotes the major crystallographic plane in which **H** was constrained to move. 1 refers to the (100) plane, 2 refers to the (001) plane, and 3 refers to the (110) plane. The superscript denotes the order of increasing size of the various extremal areas on a single branch of the Fermi surface for a major crystallographic plane. Area branches assigned to the third-band dumbbell are denoted by δ, those assigned to the fourth-band tube network are denoted by ϵ, those assigned to the fifth-band network of interconnected pear-shaped pieces are denoted by π, and those assigned to the sixth-band tooth-shaped piece are denoted by τ. The few area branches which are designated by Roman letters in Fig. 3 have been assigned to coupled orbits generated by magnetic breakdown.

IV. AREA BRANCH ASSIGNMENTS

In this section we will discuss the individual area branches and their assignment to the various sheets of the Fermi surface. The discussion will proceed from the area branches pertinent to the Fermi-surface sheets in the lowest-index Brillouin zone (the dumbbells in zone 3) to the sheets in zones of successively higher index.

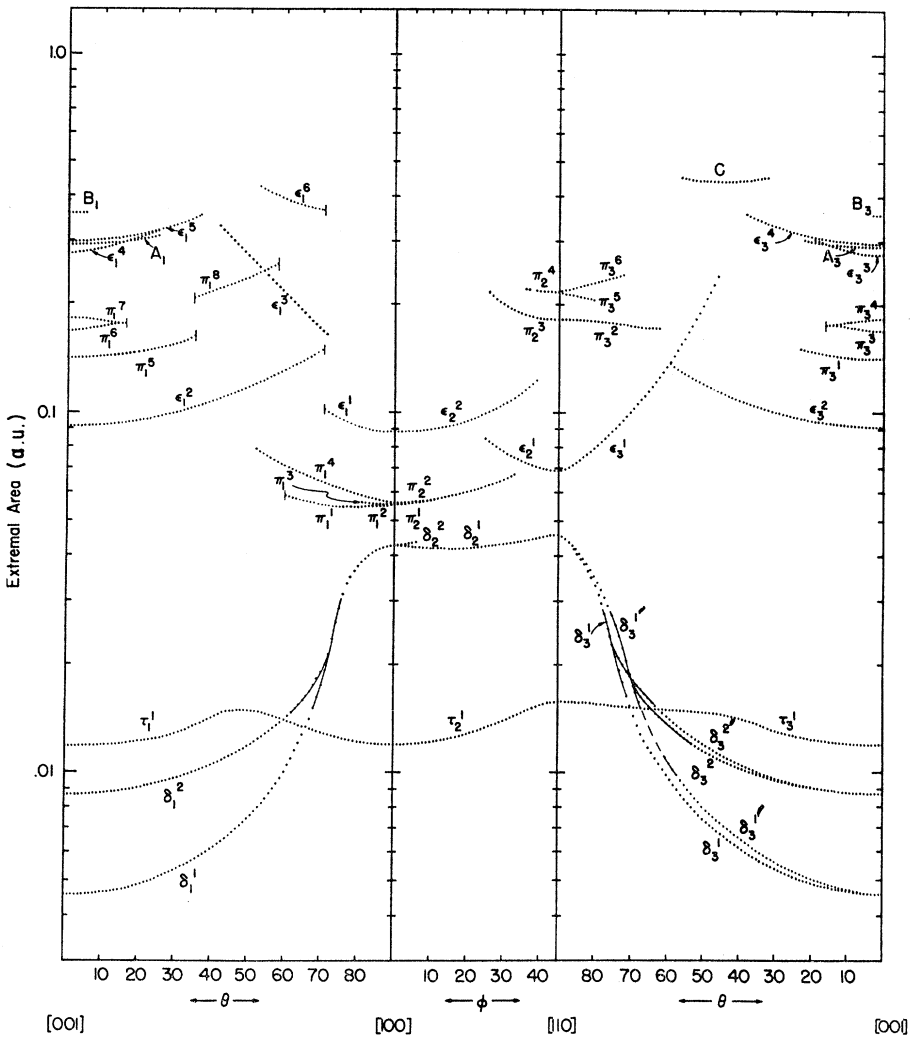

FIG. 3. A composite of all primary cross-section area branches plotted on a semilog scale in a.u. θ measures the angle between **H** and [001] in both the (100) and (110) planes. φ measures the angle between **H** and [100] in the (001) plane. A small vertical line through the termination point of any branch denotes the experimental observation of a sharp cutoff.

A. Third Zone

In this zone Weisz's model predicts the occurrence of two equivalent dumbbell-shaped pieces centered on the symmetry points X. One of these is shown in Fig. 2(a). The δ branches shown in Figs. 3 and 4 have been assigned to these sheets of the Fermi surface.

For **H** parallel to [001] ($\theta=0°$), there are two extremal areas on these dumbbells. The smallest occurs at the waist of the dumbbell in the ΓXL plane centered on the symmetry points X while the largest occurs at the heads of the dumbbell centered on the XP zone lines. The equivalent orbits δ_1^1 and δ_1^2 which give rise to these area branches are shown on the dumbbell in Fig. 2(a).

When **H** is tilted from [001] toward [100], both of the dumbbells in the third zone present identical aspects to **H**. Thus the δ_1^1 and δ_1^2 branches are both doubly degenerate. Each of these branches increases as θ increases; δ_1^1 increases more rapidly than the corresponding area change expected for a cylinder oriented along [001], while δ_1^2 increases less rapidly than expected for a cylinder. The δ_1^1 and δ_1^2 branches merge at $\theta=72.0°$. Only one branch exists for $\theta\geq 72°$; it continues to increase until it extremizes at $\theta=90°$. At the point of merger ($\theta=72°$), the δ_1^1 and δ_1^2 branches not only have the same area but also the same rate of change with θ.

When **H** is tilted from [001] toward [110], the two dumbbells in the third zone present different aspects toward **H**. Thus the double degeneracy exhibited in the (010) plane is lifted, and each fundamental branch splits into two. The δ_3^1 and $\delta_3^{2'}$ branches arise from one of these aspects while the $\delta_3^{1'}$ and δ_3^2 branches arise from the other aspect. The $\delta_3^{1'}$ and δ_3^2 branches merge at $\theta=70.0°$; the δ_3^1 and $\delta_3^{2'}$ branches merge at $\theta=74.8°$. After merger, only one branch continues for each of these sets. The branch arising from the $\delta_3^{1'}$ and δ_3^2 set was followed all the way to $\theta=90°$ at which point it extremized; the other branch was not followed for $\theta>86°$. Figure 5 shows an enlarged diagram of the

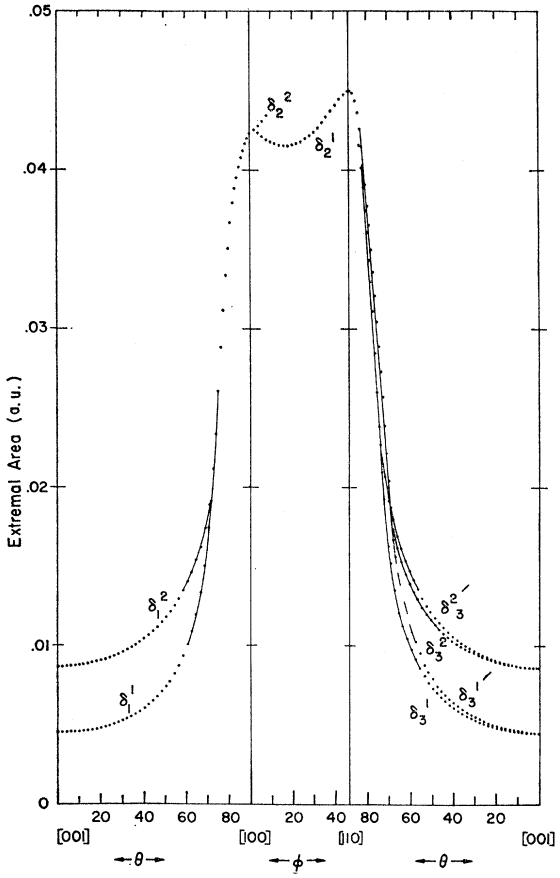

FIG. 4. Area branches assigned to extremal orbits on the third-zone dumbbells.

region where the branches merge. The $\delta_3^{1\prime}$ branch was not followed for $60.0°<\theta<67.5°$. When **H** is parallel to [110] ($\theta=90°$), the extremal cross-sectional areas occur in the ΓXP and LXP symmetry planes, respectively, of these two dumbbells. Since symmetry requires that the energy gap separating the third and fourth bands must vanish along the XP zone line (with the exception of the gap induced by spin-orbit coupling) it is reasonable to assume that the single area branch which we observe for **H** parallel to [110] measures the LXP cross section of the dumbell; the other cross section occurring in the ΓXP plane would be unobservable if magnetic breakdown[31] across the spin-orbit-coupling-induced energy gap caused a significant number of electrons to tunnel from the third to the fourth band.

The δ_2^1 area branch extremizes at $\varphi=14.5°$ and $\varphi=45°$ when **H** is rotated from [100] toward [110]. It does not extremize at $\varphi=0°$. The minimum at $\varphi=14.5°$ is consistent with the geometry of a dumbbell for which the perturbations from the free-electron model are slightly smaller than envisaged by Weisz. The minimum would be expected to occur at $\varphi\cong 9°$

[31] R. W. Stark and L. M. Falicov, in *Progress in Low Temperature Physics*, edited by C. J. Gorter (North-Holland Publishing Co., Amsterdam, 1967), Vol. V.

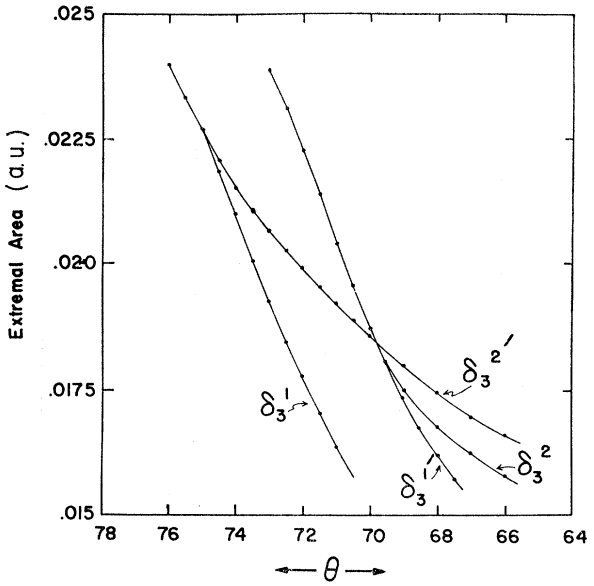

FIG. 5. Enlarged region of the third-zone area branches for **H** in the (110) plane showing the two points of merger.

on the free-electron model. The second branch which is observed splitting from δ_2^1 at [100] could not be followed for more than a few degrees beyond [100]. This branch presumably is lost due to magnetic breakdown near the XP zone line.

The experimental cross-sectional areas measured with **H** parallel to [001] are 4.59×10^{-3} and 8.68×10^{-3} atomic units (a.u.) for the δ_1^1 and δ_1^2 branches, respectively. These are to be compared with Weisz's calculated values of 3.34×10^{-3} and 8.10×10^{-3} a.u. The one experimental cross section (assumed to be in the LXP plane) for **H** parallel to [110] is 4.47×10^{-2} a.u., while the data implies that the other cross section (presumably in the ΓXP plane) is very nearly the same size. On the other hand, Weisz calculated values of 6.20×10^{-2} and 3.61×10^{-2} a.u. for these sections. It appears that he has underestimated the perturbation potential across the PXL zone plane and overestimated the potential which eliminated the interconnecting tubes from the dumbbells.

B. Fourth Zone

The area branches labeled ϵ_i^j in Fig. 3 have been assigned to the Fermi-surface sheet in the fourth zone. This sheet consists of a multiply connected set of tubes open along ΓX with a crossed convex lens-shaped reentrant region centered on Γ as shown in Figs. 2(b) and 2(c).

When **H** is parallel to [001], Weisz's model predicts the existence of four extremal orbits on this surface. Two of these occur by symmetry in the ΓXL zone plane: One going around the center crossed-lens region [the orbit labeled ϵ_1^2 in Fig. 2(c)] gives rise to the ϵ_1^2 and ϵ_3^2 area branches in Fig. 3 while the other [labeled ϵ_1^5

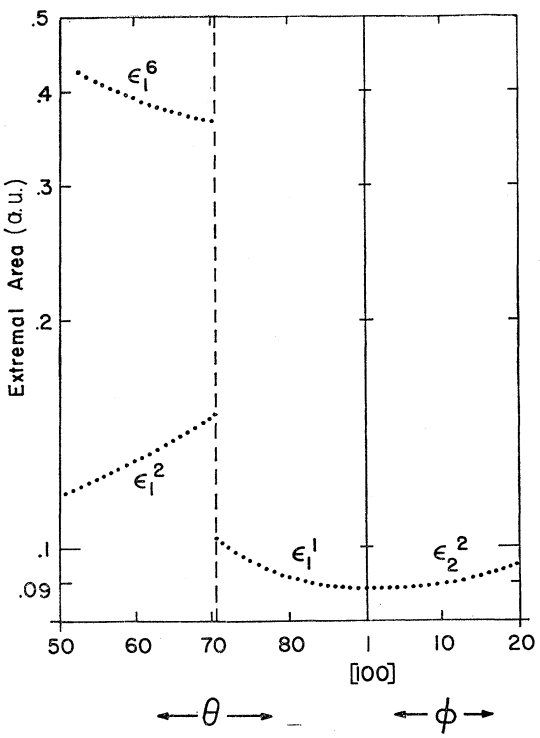

FIG. 6. Three distinct area branches which have an identical cutoff angle. This feature demonstrates that all of these are related; they have all been assigned to orbits in the fourth zone.

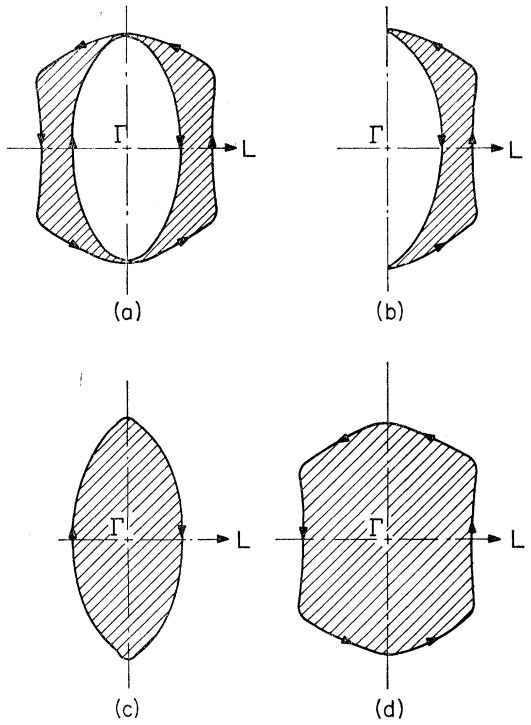

FIG. 7. The individual orbits associated with the ϵ_1^1, ϵ_1^2, and ϵ_1^6 area branches. This schematic representation of the area branches shown in Fig. 6 demonstrates the quantitative relationship between those branches at the point of cutoff: $2\epsilon_1^1+\epsilon_1^2=\epsilon_1^6$.

in Fig. 2(b)] traverses the region centered on L formed by four intersecting tubes and gives rise to the ϵ_1^5 and ϵ_3^4 area branches. The third extremal orbit [labeled ϵ_1^4 in Fig. 2(b)], centered on the LR zone line, is similar to the ϵ_1^5 orbit but occurs out of the ΓXL zone plane due to the concave curvature of the tube network. This orbit encloses an area smaller than that enclosed by ϵ_1^5 and gives rise to the ϵ_1^4 and ϵ_3^3 area branches in Fig. 3. The fourth extremal orbit [labeled ϵ_{neck} in Fig. 2(c)] is centered on the ΓH zone line and encloses the minimum area of the reentrant neck which joins the inside and outside sheets of this surface. An area branch which could be uniquely assigned to ϵ_{neck} was not observed in this experiment.

The fact that ϵ_{neck} was not observed does not, however, imply that the neck does not exist. The ϵ_1^2 branch suffered an abrupt cutoff at $\theta=70.5°$. We interpret this cutoff as evidence for the existence of the neck. This is substantiated by several other features of the data. The details of the cutoff on the ϵ_1^2 branch at $\theta=70.5°$ are shown in Fig. 6. Note that two other area branches, those labeled ϵ_1^1 and ϵ_1^6, cut off at exactly this same angle. Thus all of these must occur on this same sheet of the surface and furthermore, for our assignment, must all be centered on Γ with the ΓL zone line as a line of symmetry for their respective orbits. The ϵ_1^1 branch is assigned to the "earring" orbit described by Weisz. This orbit goes around the outside of the tube junction near Γ, across the top, and then down through the neck into the inside crossed-lens region. The ϵ_1^6 branch is assigned to the orbit centered on the ΓL zone line which goes completely around the outside of the tube junctions near Γ. This orbit (labeled ϵ_1^6) is shown in Fig. 2(b).

At $\theta=70.5°$ all three of these orbits suffer a simultaneous saddle-point cutoff. Figure 7(a) shows the central cross section of the fourth-zone surface at this critical angle where all three orbits can exist simultaneously. The individual orbits associated with the ϵ_1^1, ϵ_1^2 and ϵ_1^6 area branches at this point are shown in Figs. 7(b), 7(c), and 7(d), respectively. It is obvious that at this point these branches must satisfy the condition that $2\epsilon_1^1+\epsilon_1^2=\epsilon_1^6$. Experimentally we find that $\epsilon_1^1(70.5°)=0.102$ a.u. and $\epsilon_1^2(70.5°)=0.151$ a.u. so that the required condition yields $\epsilon_1^6(70.5°)=0.355$ a.u., which is in excellent agreement with the observed experimental value of ϵ_1^6 $(70.5°)=0.357$ a.u. Thus the character of the area branches at this cutoff verifies both the existence of the neck and the assignment of these three branches.

The ϵ_3^2 branch which is the continuation in the (110) plane of the ϵ_1^2 branch appears to cut off near $\theta=60°$. In this case we could not unambiguously determine the cutoff angle due to the presence of a much larger signal from the ϵ_3^1 branch. However, the amplitude of the ϵ_3^2 branch was decreasing quite rapidly with increasing θ when it was lost at $\theta\approx60°$. It is interesting to note that Weisz's model predicts a nearly square cross section

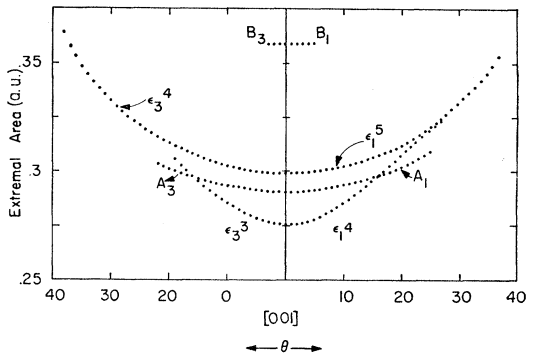

FIG. 8. Area branches assigned to orbits on the fourth-zone open tube network and magnetic-breakdown orbits between the fourth-zone tubes and third-zone dumbbells near the ΓXL zone plane.

for the neck which, if true, would lead to a predicted cutoff angle of $\theta=62.5°$ for the ϵ_3^2 branch.

The branch labeled C in the (110) plane is similar to the ϵ_1^6 branch in the (100) plane. However, in this case C results from magnetic breakdown between the third-band dumbbells and the fourth-band tube network in the vicinity of the symmetry point. The details of this magnetic breakdown will be discussed later in this paper. The amplitude of C was rather small and again it was not possible to observe an exact cutoff angle although there was some evidence that it did not terminate until $\theta\approx 60°$.

The ϵ_2^1 and ϵ_3^1 branches have been assigned to the orbit around one of the cylinders of the open tube network. An example of this orbit is shown in Fig. 2(b). The rate of increase of area with angle for both of these branches exceeds the equivalent rate of change expected for a cylinder oriented along the [110] direction and therefore must be associated with a sheet of the Fermi surface having the geometry of a hyperbolic neck oriented along the [110] axis. Thus the assignment of these area branches to the cross sections of the open tubes in the fourth band arises quite naturally.

The ϵ_1^4, ϵ_3^3, ϵ_1^5, and ϵ_3^4 area branches have all been assigned to the orbits around the inside of the open tube network as described previously. The geometry of the surface is such that as **H** is tilted away from [001] toward either [100] or [110], the smaller ϵ_1^4 and ϵ_3^3 orbits should increase more rapidly in enclosed area than the ϵ_1^5 and ϵ_3^4 orbits, respectively. One anticipates from the geometry that these two sets of branches should become degenerate and merge as θ increases. This is observed experimentally and is shown in Fig. 8. The ϵ_1^4 and ϵ_1^5 area branches merge at $\theta=30°$.

The energy gaps near the XL and XP lines of the Brillouin zone can be expected to be quite small since crystal symmetry requires that the gaps along these lines result solely from spin-orbit interactions. Hence magnetic breakdown between the third-zone dumbbells and the fourth-zone tubes is likely to have an important effect on extremal orbits which pass near the XL zone line. A considerable amount of experimental evidence

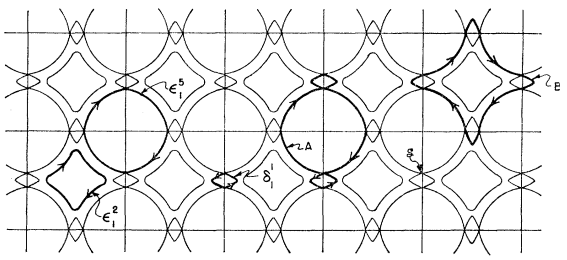

FIG. 9. Cross section in the ΓXL zone plane of the Fermi-surface sheets in the third and fourth zones shown in the repeated zone scheme. Several of the orbits which occur in the presence of magnetic breakdown are shown.

has already been accumulated for magnetic breakdown in this region[2,23,24]; our data offers further confirmation for it.

Figure 9 shows the cross section in the ΓXL zone plane of the Fermi-surface sheets in the third and fourth zones. The ϵ_1^2, ϵ_1^5, and δ_1^1 orbits previously described all occur in this plane when **H** is directed along [001]; these are shown in Fig. 9. When the magnetic-field strength becomes reasonably large ($\sim$15 kG), magnetic breakdown occurs across the spin-orbit-coupling-induced energy gap at all the points equivalent to the one labeled ζ and recouples the orbit segments of the δ_1^1 and ϵ_1^5 orbits to form new orbits. In very high fields, tunneling occurs between the third and fourth zones at every point ζ and forms the cross-shaped orbit labeled B in Fig. 9. It is apparent that the area enclosed by the B orbit is given by $B=A_{BZ}+2\delta_1^1-\epsilon_1^5$, where A_{BZ} is the cross-sectional area of the Brillouin zone ($A_{BZ}=0.6566$ a.u.). The experimental values $\delta_1^1=4.59\times10^{-3}$ and $\epsilon_1^5=0.300$ a.u. yield a predicted area for the B orbit of 0.365 a.u. This agrees reasonably well with the experimental area of 0.359 a.u. for the area branch labeled B in Figs. 3 and 8.

Additional evidence for magnetic breakdown along the LX zone line is offered by the area branch labeled A in Figs. 3 and 8 as well as the area branch labeled C in Fig. 3. Experimentally we find that when **H** is parallel to [001] the branch A satisfies the relation $A=\epsilon_1^5-2\delta_1^1$. Thus, we assign this branch to the equivalent orbit labeled A in Fig. 9. Note that in this case the orbit is formed by tunneling at some junctions while Bragg reflecting at others so that this orbit exists in the intermediate regime of magnetic breakdown for which the tunneling probability is greater than 0 but less than 1. Several other different frequencies were observed near [001] whose tentative identifications correspond to areas of $\epsilon_1^5-\delta_1^1$, $\epsilon_1^5-3\delta_1^1$, $2\epsilon_1^5$, $2\epsilon_1^5-\delta_1$, etc., but these tended to have small amplitudes and were impossible to determine with any significant accuracy.

The area branch labeled C in Fig. 3 is assigned to the orbit shown on the combined third- and fourth-zone surface in Fig. 10. If magnetic breakdown between the third and fourth zones were complete over the entire

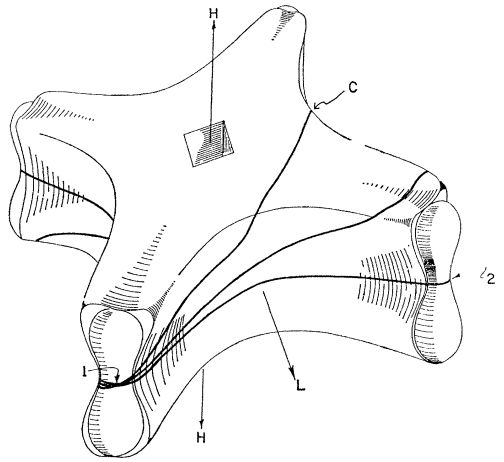

FIG. 10. The combined third- and fourth-zone Fermi surfaces. Magnetic-breakdown orbits across the spin-orbit-coupling-induced energy gap are also shown.

XLP zone faces, then branch *C* would be a continuation of branch *B*. However, the gap between these two zones is only small in the vicinity of the *XL* and *XP* zone lines. As **H** is tilted through large angles from [001] toward [110] the extremal orbit will pass near the *XL* lines for only one set of dumbbell-tube junctions (the junction labeled "1" in Fig. 10). Thus, the extremal orbit will tend to undergo magnetic breakdown near the "1" junctions even for large values of θ. The *B* orbits where only observed for $\Theta \lesssim 5°$. This indicates that magnetic breakdown is only prevalent for a distance of 0.035 a.u. above and below *X* measured parallel to the *XP* line. Thus, when $\Theta \gtrsim 5°$, magnetic breakdown near "2" is no longer probable so that the likelihood of forming a *B* orbit becomes vanishingly small. As θ is increased the orbit plane near "2" eventually cuts the dumbbell near its tip along the *XP* line. In this region the gap is again expected to be small and magnetic breakdown again becomes likely, leading to the orbit labeled *C* in Fig. 10. Weisz's model predicts that the *C* branch will first become observable for $\Theta \approx 33°$; experimentally the onset occurs at $\theta = 32°$. Weisz's model also predicts that the *C* orbit should be cut off at $\Theta \approx 60°$ by the neck region. In addition, the size and variation with θ of the *C* branch agreed reasonably well with Weisz's model.

Thus, all of the observed area branches which we have assigned to the fourth zone sheet of the Fermi surface confirm the qualitative predictions of Weisz's model if we include the effects of magnetic breakdown. Quantitatively, however, the agreement is not very good, as is shown in Table I which lists the values of the experimental area branches for various directions of **H** together with values calculated by Weisz.

C. Fifth Zone

The area branches labeled π_i^j in Fig. 3 have been assigned to the Fermi-surface sheet in the fifth zone.

TABLE I. Area branch values for particular directions of **H**.

Symbol	Coordinates of **H** θ	φ	Crystalline axis	Expt. areas (a.u.)	Calc. areas (Weisz) (a.u.)
$\delta_1^1, \delta_3^1, \delta_3^1$	0		[001]	4.59×10^{-3}	3.34×10^{-3}
$\delta_1^2, \delta_3^2, \delta_3^2$	0		[001]	8.68×10^{-3}	8.10×10^{-3}
$\epsilon_1^2, \epsilon_3^2$	0		[001]	(9.11×10^{-2})	1.15×10^{-1}
$\epsilon_1^4, \epsilon_3^3$	0		[001]	2.76×10^{-1}	
$\epsilon_1^5, \epsilon_3^4$	0		[001]	3.00×10^{-1}	3.19×10^{-1}
A_1, A_3	0		[001]	2.90×10^{-1}	
B_1, B_3	0		[001]	3.59×10^{-1}	3.58×10^{-1}
π_1^5, π_3^1	0		[001]	(1.41×10^{-1})	1.519×10^{-1}
π_1^6, π_3^2	0		[001]	1.69×10^{-1}	
π_1^7, π_3^4	0		[001]	1.82×10^{-1}	2.17×10^{-1}
τ_1^1, τ_3^1	0		[001]	1.19×10^{-2}	7.5×10^{-3}
$\delta_1^1, \delta_2^1, \delta_2^2$	90°	0	[100]	(4.22×10^{-2})	
$\epsilon_1^1, \epsilon_2^2$	90°	0	[100]	(8.80×10^{-2})	8.41×10^{-2}
$\pi_1^1, \pi_1^3, \pi_2^1$	90°	0	[100]	(5.51×10^{-2})	7.37×10^{-2}
$\pi_1^2, \pi_1^4, \pi_2^2$	90°	0	[100]	(5.58×10^{-2})	
τ_1^1, τ_2^1	90°	0	[100]	1.20×10^{-2}	1.87×10^{-2}
δ_3^1, δ_2^1	90°	45°	[110]	(4.47×10^{-2})	3.61×10^{-2}
$\epsilon_2^1, \epsilon_3^1$	90°	45°	[110]	(6.84×10^{-2})	6.20×10^{-2}
$\pi_2^4, \pi_3^5, \pi_3^6$	90°	45°	[110]	1.81×10^{-1}	
π_2^3, π_3^2	90°	45°	[110]	(2.15×10^{-1})	
τ_2^1, τ_3^1	90°	45°	[110]	1.57×10^{-2}	
τ_1^1	48.0°	0	[110]	1.49×10^{-2}	
π_1^1, π_1^2	87.0°	0	[110]	(5.46×10^{-2})	
δ_2^1	90°	14.5°		(4.13×10^{-2})	
C	44.0°	45°		4.43×10^{-1}	

This sheet, as shown in Fig. 2(d), consists alternately of top-up and top-down pear-shaped pieces interconnected by a network of tilted tubes. The geometry of these is essentially the same for both the free-electron model and for Weisz's model.

When **H** is parallel to [001] one expects to observe three different area branches arising from this surface. One of these results from an orbit enclosing maximum area about the largest part of the top of the pear [orbit π_1^7 in Fig. 2(d)], a second results from an orbit enclosing minimum area about the base of the pear just above the region where it junctions with the tilted tubes [orbit π_1^6 in Fig. 2(d)], and a third results from an orbit about the inside of the network of tilted tubes [orbit π_1^5 in Fig. 2(d)]. The area branches labeled π_1^5, π_3^1, π_1^6, π_3^3, π_1^7, and π_3^4 have been assigned to these orbits.

When **H** is tilted away from [001] toward either [100] or [110] one observes that π_1^6 and π_3^3 merge with the π_1^7 and π_3^4 area branches, respectively. Both sets of area branches cut off at the exact point of merger. This is precisely the type of behavior expected for the π_1^6 and π_1^7 orbits since the minimum π_1^6 orbit is effectively pinned down by the saddle-point character of the junction region between the tilted tubes and the pear-shaped piece.

The cross-sectional areas of this surface measured in planes perpendicular to **H** are shown plotted in Fig. 11 as a function of position measured parallel to **H**. These are shown for three different values of θ; θ_1 corresponds

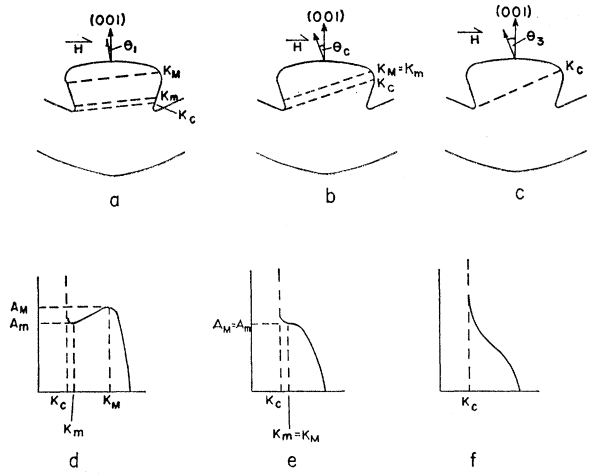

FIG. 11. Cross-sectional areas of the fifth-band pear surface measured in planes perpendicular to **H** as a function of position measured parallel to **H**. (a), (b), and (c) show the positions on the surface of the extremal orbits (labeled K_m and K_M) and the saddle-point orbit (labeled K_c). (c), (d), and (f) show the extremal area variations, respectively, for $\theta=\theta<\theta_c$, $\theta=\theta_c$, and $\theta=\theta_3>\theta_c$.

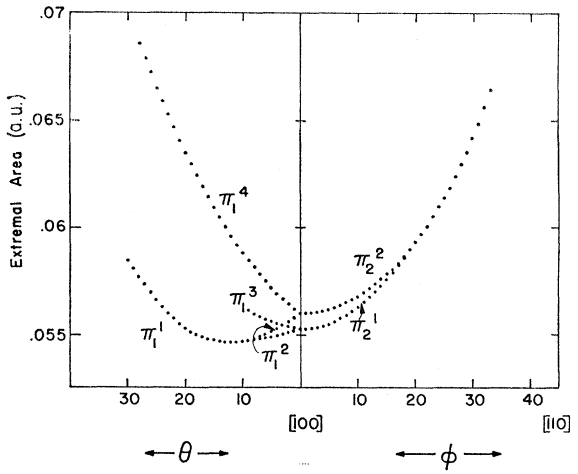

FIG. 12. Enlarged region showing the area branches assigned to orbits around the connecting tubes of the fifth zone.

to an angle sufficiently small that both maximum and minimum areas exist, θ_c corresponds to the critical angle for which the maximum and minimum areas merge, and $\theta_3>\theta_c$. The most important feature of each of these area plots is the discontinuity that occurs at the saddle-point location K_c. For $\theta=\theta_c$ the extremal area occurs at the stationary point on the curve. For $\theta>\theta_c$ there is no extremal area.

The π_1^5 and π_3^1 area branches have been assigned to orbits around the inside of the tilted tube network. When **H** is tilted from [001] toward [100] the π_1^5 area branch increases slowly with θ until it cuts off at $\theta=35°$. The π_3^1 area branch which is the continuation in the (110) plane of the π_1^5 area branch suffers a cutoff at $\theta\approx23°$.

The π_1^1, π_1^2, π_1^3, π_1^4, π_2^1, and π_2^2 area branches shown in Fig. 3 and in an enlarged diagram in Fig. 12 have been assigned to orbits around the tilted tubes [orbits π_2^1 and π_2^2 in Fig. 2(d) and orbit π_1^1 in Fig. 13(c)]. It is apparent from the data shown in Fig. 12 that when **H** is along [100] these tubes have both minimum (π_2^1) and maximum (π_2^2) extremal cross-sectional areas. As **H** is tilted from [100] toward [110], the π_2^1 and π_2^2 area branches merge at $\varphi=21.0°$, and as **H** is tilted from [100] toward [001] the π_1^1 and π_1^2 area branches merge at $\theta=77°$, the point at which these branches have minimum area. This indicates that these tubes are tilted about 13° toward [001] from [100] in accord with the tilt angle predicted by Weisz's model. The π_1^1 branch was observed to cut off at $\theta\approx59°$. No cutoff was observed for the π_1^4 branch; its signal amplitude decreased slowly into the noise as **H** was tilted from [100] toward [001].

The π_1^8 area branch was observed to cut off sharply at each of its ends. These cutoffs occurred at $\theta=35°$ and $\theta=59°$. Notice that the first cutoff occurs at exactly the same angle as the cutoff on the π_1^5 branch and that the second cutoff occurs at exactly the same angle as the cutoff on the π_1^1 branch. This relationship immediately serves to identify the orbit which gives rise to the π_1^8 area branch. In addition, it proves explicitly that the π_1^5, π_1^8, π_1^1, π_1^2, π_1^3, and π_1^4 area branches all arise from the same sheet of the Fermi surface. The types of orbits which give rise to the π_1^5, π_1^8, and π_1^1 area branches are shown in Figs. 13(a), 13(b), and 13(c). Notice that all three of these orbits have a common center line of symmetry (a twofold rotation axis labeled X-X) about which the orbit plane tilts as θ is increased.

The area branches labeled π_2^3 and π_2^4 have been assigned to extremal orbits about the pear-shaped section of the surface. The equivalent orbits are shown on the surface in Fig. 2(d). The π_2^3 orbit encloses minimum area about the pear whereas the π_2^4 orbit encloses maximum area about the pear and part of the tilted tubes. The π_3^5 and π_3^6 area branches do not extremize at $\theta=90°$ in accord with this assignment.

The experimental values of all of the π area branches for **H** along symmetry directions are listed in Table I together with those values given by Weisz for his model. The qualitative behavior of all of these area branches agrees well with the predictions of Weisz's model but, as was the case for the area branches assigned to sheets of the Fermi surface in zones 3 and 4, the quantitative agreement of the experimental areas with Weisz's model is not very good.

D. Sixth Zone

Weisz's model predicts two equivalent sheets of the Fermi surface in the sixth Brillouin zone. These are centered at the points labeled W in Fig. 1 and have the shape of an extracted tooth as shown in Fig. 2(e). We have assigned the area branch labeled τ in Fig. 3 to this sheet of the Fermi surface.

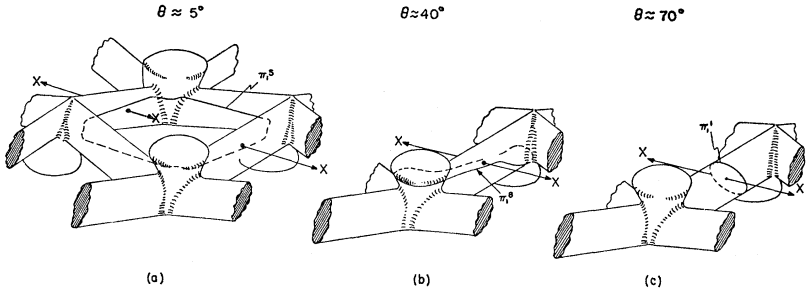

FIG. 13. Orbits on the fifth-zone sheet of the Fermi surface which give rise to the π_1^5, π_1^8, and π_1^1 area branches: (a) π_1^1 hole orbit inside tube network; (b) π_1^8 electron orbit; (c) π_1^1 electron orbit. All three orbits have the common X-X center line of symmetry.

Although only one single branch is shown for τ in Fig. 3, there was clear evidence for other branches running near this one. We have not as yet, however, been able to sort these other branches from the one shown. The size and variation with angle of the τ branches are qualitatively consistent with a sheet of the Fermi surface shaped like Weisz's sixth-band surface. However, it appears that the actual Fermi-surface sheet that gives rise to the τ branches is somewhat smaller and more isotropic than Weisz's. In particular, it appears that the roots of the tooth-shaped surface are somewhat more diminutive than Weisz's model. The actual geometry of this piece of the surface cannot be uniquely defined until we have completed sorting of the remaining branches near τ.

E. Unassigned Area Branch

The only area branch for which we have been unable to find an unambiguous assignment is the one labeled ϵ_1^3 in Fig. 3. There appears to be only one orbit which is capable of explaining the existence of ϵ_1^3, an orbit which goes around the outside of the fourth-zone tube network, down through the reentrant neck, and then traverses the inside cross-lens region. This orbit would be noncentral and would look like two of the earring orbits shown in Fig. 7(b) joined at one side only. This assignment should be regarded as tentative and must await the results of a detailed band-structure calculation for final verification.

V. CONCLUSIONS

The experimental data which we have reported in this paper demonstrates a remarkable degree of qualitative consistency with the predictions of Weisz's Fermi-surface model for white tin. The quantitative agreement, however, is not very good; in fact, the disagreements are large enough to warrant new band-structure calculations. These calculations are currently being carried out and will be the subject of a future paper.

One should note that the de Haas–van Alphen frequency branches reported in this paper only constitute a subset of the total frequency branches which were observed. We did not report the remaining frequency branches simply because we were able to show quite unambiguously that in every case these resulted either from harmonics of branches reported or were exact sum and difference frequency branches resulting from nonlinear combinations of two of the branches reported. Several of these nonlinear branches have been reported by other investigators[1,2]; attempts to assign these to fundamental orbits on the Fermi surface have resulted in some confusion.

Magnetic breakdown between the third-band dumbbell and the fourth-band tube network has been observed to occur in the regions of both the XL and XP zone lines where the energy gaps separating these two bands result solely from spin-orbit interactions. No evidence was obtained in the course of these investigations which indicated that magnetic breakdown occurred at any other region of the Fermi surface.